

1 **Arabidopsis SYT1 Maintains Stability of Cortical ER Networks and**
2 **VAP27-1-Enriched ER-PM Contact Sites**

3

4 **Wei Siao¹, Pengwei Wang², Boris Voigt¹, Patrick J. Hussey² and Frantisek**
5 **Baluska¹**

6 ¹Institute of Cellular and Molecular Botany, University of Bonn, Kirschallee 1
7 D-53115 Bonn, Germany

8 ²School of Biological and Biomedical Sciences, Durham University, South Road,
9 Durham, DH1 3LE, UK

10

11 **Running Title:** Arabidopsis SYT1 and VAP27-1 on Distinct ER-PM Contact Sites

12

13 **Author E-mail**

14 Wei Siao: siao@uni-bonn.de

15 Penwei Wang: pengwei.wang@durham.ac.uk

16 Boris Voigt: bvoigt@uni-bonn.de

17 **Corresponding Author E-mail and Telefon**

18 Frantisek Baluska: unb15e@uni-bonn.de; +49 228 734761

19 Patrick J. Hussey: p.j.hussey@durham.ac.uk; +44 191 33 41017

20

21 **Date of Submission:** 23 July, 2016.

22 **Number of Tables and Figures:** 1 Table and 7 Figures. (Figure 1, 2 and 3 should
23 colour in print; all figures should be colour online.)

24 **Word Count:** 4248.

25 **Number of Supplementary Data:** 4 Supplementary Figures and 4 Supplementary
26 Movies.

27

28

29

30

31

32

33

34 **Highlight**

35 Arabidopsis synaptotagmin 1 is localized on the ER-PM contact sites distinct from
36 VAP27-1 and plays roles in maintaining ER morphology and the dynamic of VAP27-
37 1.

38

39 **Abstract**

40 Arabidopsis synaptotagmin 1 (SYT1) is localized on the endoplasmic reticulum-
41 plasma membrane (ER-PM) contact sites in leaf and root cells. The ER-PM
42 localization of Arabidopsis SYT1 resembles that of the extended synaptotagmins (E-
43 SYTs) in animal cells. In mammals, E-SYTs have been shown to regulate calcium
44 signaling, lipid transfer, and endocytosis. Arabidopsis SYT1 was reported to be
45 essential for maintaining cell integrity and virus movement. This study provides
46 detailed insight into the subcellular localization of SYT1 and VAP27-1, another ER-
47 PM tethering protein. SYT1 and VAP27-1 were shown to be localized on distinct ER-
48 PM contact sites. The VAP27-1-enriched ER-PM contact sites (V-EPCSs) were
49 always in contact with the SYT1-enriched ER-PM contact sites (S-EPCSs). The V-
50 EPCSs still existed in the leaf epidermal cells of *SYT1* null mutant; however, they
51 were less stable than that in the wild type. The polygonal networks of cortical ER
52 disassembled and the mobility of VAP27-1 protein on the ER-PM contact sites
53 increased in leaf cells of *SYT1* null mutant. These results suggest that SYT1 is
54 responsible for stabilizing ER network and V-EPCSs.

55

56 **Key Words:** Synaptotagmins, VAP27, ER-PM Contact Sites, Cortical ER, ER
57 Stability, Cytoskeletons, Protein Dynamics.

58

59 **Introduction**

60 In eukaryotic cells, proteins with multiple C2 domains are often found to participate
61 in membrane trafficking or membrane tethering processes, which can likely be Ca²⁺-
62 regulated (Nalefski and Falke, 1996; Min *et al.*, 2007). Arabidopsis Synaptotagmin 1
63 (SYT1) belongs to a five-member gene family (SYT1-5), all of which contain an N-
64 terminal transmembrane domain (TM), a synaptotagmin-like mitochondrial and lipid-
65 binding protein (SMP) domain, and two tandem C2 domains at its C-terminus
66 (Yamazaki *et al.*, 2010). The protein structure of Arabidopsis SYT1 is similar to both
67 synaptotagmins (SYTs) and extended synaptotagmins (E-SYTs) in metazoan (Craxton,

68 2010).

69

70 At least 17 SYT isoforms have been found in mammals, most of them are expressed
71 in neurons or neuroendocrine cells, and play essential roles in Ca^{2+} -regulated
72 neurotransmission and hormone secretion (Moghadam and Jackson, 2013). On the
73 other hand, mammalian E-SYTs are ER membrane proteins that have similar
74 functional domains as plant homologues (Min *et al.*, 2007). Human *E-SYT1* is
75 expressed almost ubiquitously while human *E-SYT2* and *E-SYT3* are expressed mainly
76 in cerebellum (Min *et al.*, 2007). Mammalian E-SYTs are known to participate in the
77 ER-PM tethering (Stefan *et al.*, 2013).

78

79 Several proteins localized on the ER-PM contact sites (EPCSs) in plants are reported
80 recently, including Networked 3C (NET3C), VAMP/synaptobrevin-associated protein 27
81 (VAP27)-1, -3 and -4 (VAP27-1, VAP27-3 and VAP27-4), and synaptotagmin 1 (SYT1).
82 NET3C belongs to the plant-specific NET superfamily of actin binding proteins. All
83 the 13 members of the Arabidopsis NET family contain a NET actin-binding (NAB)
84 domain and various numbers of coiled-coil domains that can simultaneously interact
85 with the actin filaments and different membrane compartments (Deeks *et al.*, 2012;
86 Hawkins *et al.*, 2014; Wang *et al.*, 2014). Arabidopsis VAP27 proteins belongs to the
87 VAP33-like family which are homologs of mammalian VAPs and yeast suppressor of
88 choline sensitivity (Scs2) (Sutter *et al.*, 2006; Saravanan *et al.*, 2009). The conserved
89 major sperm (MSP) domain is essential for VAP27-1 to anchor on the ER-PM contact
90 sites and interaction of VAP27-1 with NET3C.

91

92 Arabidopsis SYT1 was thought to be a PM protein but recent studies, as well as our
93 result here have shown that it is an ER-resident protein (Perez-Sancho *et al.*, 2015).
94 Arabidopsis *SYT1* is constitutively expressed in all the tissues and the mutants are more
95 sensitive to salt, freezing and mechanical stresses (Schapire *et al.*, 2008; Yamazaki *et*
96 *al.*, 2008; Yamazaki *et al.*, 2010; Levy *et al.*, 2015; Perez-Sancho *et al.*, 2015). In
97 addition, the virus infections are delayed in *SYT1* null mutant (Lewis and Lazarowitz,
98 2010; Uchiyama *et al.*, 2014). Arabidopsis SYT1 and VAP27-1 have also been shown
99 to interact with the plasmodesmata-resident reticulons (Kriechbaumer *et al.*, 2015).
100 However, the relationship between Arabidopsis SYT1 and VAP27-1 on the ER-PM
101 contact sites is still unclear.

102

103 This work addresses the spatial relationships between Arabidopsis SYT1, VAP27-1
104 and microtubules on the cell cortex. By live-cell imaging, immunocytochemistry, and
105 immunogold labeling, SYT1 and VAP27-1 are shown to be localized on distinct ER-
106 PM contact sites. V-EPCSs are always in contact with S-EPCSs and often associated
107 with microtubules, but S-EPCSs are often excluded by microtubules on the cell cortex
108 and often arranged along thick actin filaments. Amino acid substitutions demonstrate
109 that VAP27-1 mutant protein has no dominant-negative effect on the SYT1 anchoring
110 to the PM. Using stable transformation of VAP27-1 in Arabidopsis, SYT1 is shown to
111 be essential for maintaining the stability of ER network and the ER-PM contact sites.
112 The dynamic of VAP27-1 on the ER-PM contact sites is restrained by SYT1. In
113 summary, this study shows that Arabidopsis SYT1 is critical for tethering the ER to
114 the PM and plays roles in regulating the ER remodelling and the stability of V-EPCSs.
115

116 **Material and Methods**

117 ***Plant Material and Growth Conditions***

118 *Arabidopsis thaliana* (L.) seedlings were grown on vertical half-strength Murashige
119 and Skoog (1/2 MS) agar plates (pH = 5.8) in a growth chamber at 22°C under long-day
120 conditions (16 h Light/ 8 h Dark). After 14 days, the seedlings were transfer and grown in
121 pots in a culture room at 22°C under long-day conditions (16 h Light/ 8 h Dark).
122 Experiments were performed using *Arabidopsis thaliana* Columbia ecotype (Col-0),
123 *syt1-2* (SAIL_775_A08), *SYT1 promoter:SYT1-GFP/Col-0* transgenic line (Yamazaki
124 *et al.*, 2010), *VAP27-1* RNAi knock-down lines and *VAP27-1-YFP/Col-0* transgenic
125 lines (Wang *et al.*, 2014; Wang *et al.*, 2016). *VAP27-1-YFP/syt1-2* transgenic lines were
126 obtained by Agrobacterium-mediated transformation of *VAP27-1-YFP* into *syt1-2*
127 using floral-dipping (Clough and Bent, 1998; Zhang *et al.*, 2006). For FM4-64
128 staining and BFA treatment, roots of 4-day-old Arabidopsis seedlings were transferred
129 into 1/10 MS solution and pre-cooled at 6°C for 5 min. After stained with 4.1 μM of
130 FM4-64 (SynaptoRed™ C2, Sigma) at 6°C for 10 min, the roots were incubated with
131 35.6 μM of BFA at room temperature for 60 min. Z-stack images of the roots at 2 μm
132 intervals were acquired by confocal microscopy.

133

134 ***Constructs***

135 Binary plasmids of Arabidopsis SYT1 tagged with GFP driven by native *SYT1* promoter

136 (SYT1-GFP), VAP27-1 tagged with YFP driven by 35S promoter (VAP27-1-YFP),
137 and NET3C fused with RFP driven by 35S promoter (RFP-NET3C) were described
138 previously (Yamazaki *et al.*, 2010; Wang *et al.*, 2014). The ER marker RFP-HDEL
139 and CFP-HDEL (Lee *et al.*, 2013; Wang *et al.*, 2014), the Golgi marker ST-RFP
140 (Renna *et al.*, 2005; Schoberer *et al.*, 2010), the early endosome marker CLC-mCherry
141 (Wang *et al.*, 2015; Wang *et al.*, 2013), the microtubule marker MBD-MAP4-DsRed
142 (Marc *et al.*, 1998; Granger and Cyr, 2001), and the actin maker ABD2-mCherry
143 (Voigt *et al.*, 2005) were described in the indicated reports.

144

145 ***Agrobacterium-mediated Transient Expression in Tobacco Leaves***

146 *Nicotiana benthamiana* plants were grown in a culture room at 22°C under long-day
147 conditions (16 h light/8 h dark) for 3-4 weeks. Each construct was transformed into
148 *Agrobacterium tumefaciens* strain GV3101::pMP90 by electroporation followed by
149 selection on YEB plates containing the appropriate antibiotics. Single colony was
150 inoculated and grown overnight in 3 ml YEB liquid medium with antibiotics at 37°C.
151 1 ml of bacterial culture was centrifuged at 3,500 rpm for 5 min and the pellet was
152 resuspended in 1 ml of infiltration medium (20 mM citric acid, 2% sucrose and 0.2
153 mM acetosyringone). The bacterial suspension was centrifuged and the pellet was
154 resuspended again in 1 ml of infiltration medium to ensure complete removal of
155 remnant antibiotics. Absorbance of the suspension at 600 nm was measured and
156 the OD₆₀₀ was adjusted to the specified value for infiltration (OD₆₀₀ = 0.2 for SYT1-
157 GFP, CLC-mCherry, MAP4-DsRed and ABD2-mCherry; OD₆₀₀ = 0.1 for VAP27-1-
158 YFP, NET3C-RFP, ST-RFP, RFP-HDEL and CFP-HDEL). Syringe infiltration of
159 tobacco leaves was performed as previously described (Batoko *et al.*, 2000; Sparkes *et*
160 *al.*, 2006). The plants were kept in the same culture room after infiltration for 2 days
161 before confocal imaging. The PM staining was conducted by infiltrating 4.1 μM of
162 FM4-64 (SynaptoRed™ C2, Sigma) in Milli-Q water into the leaves 5 min prior to
163 microscopy.

164

165 ***FRAP Analysis***

166 Stable transgenic Arabidopsis expressing VAP27-1-YFP in Col-0 (*VAP27-1-YFP/Col-*
167 *0*) and *syt1-2* (*VAP27-1-YFP/syt1-2*) background were grown in pots for 4 weeks. One
168 T3 homozygous line of VAP27-1/Col-0 and five T1 heterozygous lines of VAP27-
169 1/*syt1-2* were planted. The expression levels of VAP27-1-YFP in five VAP27-1/*syt1-2*

170 heterozygous lines were examined by confocal microscope, and one with comparable
171 expression of VAP27-1-YFP with that in VAP27-1/Col-0 was used for FRAP
172 experiments. Leaf discs (0.5 x 0.5 cm²) from the first or second leaf of the 4-week-old
173 Arabidopsis were selected because the leaves have flattened surface. The leaf discs
174 were mounted in Milli-Q water and analyzed using confocal microscope with a 60x
175 oil immersion objective and a zoom factor of 5.0. Confocal parameters were identical
176 for all the FRAP experiments. 2% transmission of an argon laser at 515 nm was used
177 for imaging and 80% transmission for photobleaching. Ten reference scans were taken
178 before bleaching and 60 scans were taken after bleaching at 3-sec intervals. At least
179 20 VAP27-1-YFP-labeled puncta in each line were analyzed. The raw data were
180 normalized and the best-fit curves were generated by least-squares regression using
181 Prism (Graumann *et al.*, 2007; Wang *et al.*, 2011).

182

183 ***Western Blot***

184 14-day-old seedlings were frozen by liquid nitrogen and grounded into powder. The
185 total protein was extracted with protein extraction buffer (50 mM Tris-HCl, 150 mM
186 NaCl, 10 mM MgCl₂, 0.5 % NP-40, 1 mM PMSF and 1 X protease inhibitor cocktail
187 (P9599, Sigma). The protein samples were quantified using Bio-Rad Bradford Protein
188 Assay and subjected to 5X sample buffer (300 mM Tris-HCl, 60% Glycerol, 10%
189 SDS, 500 mM DTT and 0.01% bromphenol blue). The protein was denatured by
190 heating at 70°C for 5 min and cooled down on ice. 40 µg of protein was loaded to gels
191 for SDS-PAGE analysis and transferred onto a PVDF membrane by eletroblotting.
192 The membranes were first stained with Ponceau S, imaged and then blocked with 4%
193 non-fat milk + 4% BSA in Tris-buffered saline with Tween 20 (TBST; 10 mM Tris,
194 150 mM NaCl and 0.1% Tween 20, pH 7.6) for 60 min. After incubation with
195 antibodies against SYT1 (1:1000) or VAP27-1 (1:1500) at 4°C for 16 h, the membranes
196 were washed three times for 10 min and incubated with HRP-conjugated anti-rabbit or
197 HRP-conjugated anti-mouse antibodies at room temperature for 1.5 h. The blots were
198 washed three times with TBST for 10 min, and the proteins were visualized using
199 ECL imaging system (LAS-1000, Fuji Films). SYT1 antibody was kindly provided by
200 Prof. Miguel A. Botella, Universidad de Malaga, Spain (Perez-Sancho *et al.*, 2015),
201 and VAP27-1 anti-serum was described previously (Wang *et al.*, 2014; Wang *et al.*,
202 2016).

203

204 ***Immunogold Labeling***

205 Root tips of Arabidopsis, with or without pre-treatment of 50 μ M BFA for 2 h, were
206 fixed using a high-pressure freezing machine (Bal-Tec HPM010, Balzers, Liechtenstein),
207 freeze-substituted at -80°C and embedded in Lowicryl® Embedding Media HM20
208 (Polysciences, Warrington PA). After blocked and incubated with antibodies against
209 SYT1 (1:150) and VAP27-1 (1:150) overnight at 4°C, the ultrathin sections were
210 rinsed and incubated with 15-nm gold particle-conjugated anti-rabbit and 6-nm gold
211 particle-conjugated anti-mouse antibodies at room temperature for 2 h. The sections
212 were extensively washed and stained with uranyl acetate. The samples were imaged
213 with an LEO 912AB electron microscope (ZEISS AG, Oberkochen). For statistical
214 analysis, the positive gold signals were counted along the PM (within a distance of 50
215 nm apart from the PM). A region of interest (ROI) was defined as a rectangle area with
216 a width of 50-nm (apart from the PM) and a length of 100-nm along the PM. More than
217 one positive signal within a ROI was defined as a clustered labeling (co-localization).
218

219 ***Whole Mount Immunofluorescence Labeling***

220 5-day-old Arabidopsis seedlings were fixed in fixation buffer (1.5% paraformaldehyde +
221 0.5% glutaraldehyde in 1/2 microtubule stabilizing buffer (MTSB; 50 mM PIPES, 5 mM
222 MgSO₄ and 5 mM EGTA, pH 6.9) with vacuum filtration for 1 h, and the fixed
223 seedlings were washed once with 1/2 MTSB and twice with phosphate-buffered saline
224 (PBS; 140 mM NaCl, 2.7 mM KCl, 6.5 mM Na₂HPO₄ and 1.5 mM KH₂PO₄, pH 7.3)
225 for 10 min. After three times of reduction with sodium borohydride (NaBH₄) in PBS,
226 the roots were washed three times for 5 min and then incubated with 2% driselase +
227 2% cellulose + 1% pectolyase in PBS at 37°C for 30 min. The cells were permeabilized
228 by incubating with 10 mM glycine three times for 5 min and 2% Nonidet P40 + 10%
229 DMSO for 1 h in PBS. The roots were washed with PBS for 10 min and then blocked
230 with 2% BSA in PBS. After incubation with antibodies against SYT1 (1:200) and
231 VAP27-1 (1:200) at 4°C for 16 h, the roots were washed six times for 10 min and
232 incubated with Cy5®-conjugated anti-rabbit and Alexa Fluor® 488-conjugated anti-
233 mouse antibodies at 37°C for 1.5 h plus at room temperature for 1.5 h. For single
234 SYT1 immunolabeling, Alexa Fluor® 488-conjugated anti-rabbit antibody was used.
235 The roots were washed six times for 10 min, and the nuclei were stained with 5 μ M
236 DAPI in PBS. The roots were washed twice with PBS for 5 min before confocal imaging.
237

238 **Confocal Microscopy**

239 Confocal imaging was performed by using an Olympus FluoView™ FV1000 confocal
240 microscope equipped with diode (405 nm), argon-ion (458, 488 and 514nm) and
241 helium–neon (543nm) lasers. GFP single image was excited at 488 nm and the emission
242 signals were collected from 500nm to 600nm. YFP was excited at 515 nm and emission
243 was collected from 530nm to 630nm. The red fluorescent dye FM4-64 was excited at
244 543 nm and emission was filtered between 660 and 760nm. For simultaneous imaging
245 of CFP, GFP and FM4-64 the setting of CFP (Ex 405nm/Em 440-505nm), GFP (Ex
246 488nm/Em 510-550 nm) and FM4-64 (Ex 543 nm/Em 600-660nm) was used. For
247 simultaneous imaging of GFP, YFP and mCherry the setting of GFP (Ex 458nm/Em
248 470-515nm), YFP (Ex 514nm/ Em 530-580nm) and mCherry (Ex 543 nm/Em 600-
249 660nm) was used.

250

251 **Accession Numbers**

252 *Arabidopsis* *SYT1* (AT2G20990); *VAP27-1* (AT3G60600); *NET3C* (AT2G47920)

253

254 **Results**

255 ***Arabidopsis* SYT1 is localized on the ER-PM contact sites**

256 *Arabidopsis* Synaptotagmin 1 (SYT1) and VAP27-1 have been shown to be ER-PM
257 tethering proteins. However, the relationship between SYT1 and VAP27-1 remains
258 unclear. To gain a better understanding this relationship, SYT1-GFP was first
259 transiently co-expressed with the ER lumen markers RFP-HDEL or CFP-HDEL in
260 leaves of *Nicotiana benthamiana*. Most SYT1-GFP signals were found to accumulate
261 on stable spots along the relatively stationary ER tubules and cisternae while less
262 amount of SYT1-GFP was detected on the motile, quickly remodeling ER strands
263 (Fig. 1A and Supplementary Movie S1). The co-expression of CFP-HDEL followed
264 by FM4-64 staining showed that SYT1-GFP was localized on the ER and attached to
265 the PM at specific stationary regions, i.e., the ER-PM contact sites (Fig. 1B and 1C).
266 This observation is in agreement with previous studies (Levy *et al.*, 2015; Perez
267 Sancho *et al.*, 2015) and immunogold labeling of endogenous proteins (discussed
268 later).

269

270 Studies have shown that *Arabidopsis* SYT1 plays roles in regulating the endocytosis
271 in the leaves of *N. benthamiana* (Lewis and Lazarowitz, 2010) and the secretory

272 pathway in *Arabidopsis* (Kim *et al.*, 2016). However, the functions of SYT1 on the
273 endocytic pathway in *Arabidopsis* remain unclear. To investigate whether SYT1
274 would be incorporated in the endocytic vesicles, SYT1-GFP was co-expressed with
275 the Golgi marker (ST-RFP) and the early endosome marker (CLC-mCherry). The
276 results showed that SYT1 was not translocated into the Golgi apparatus and the
277 clathrin-coated vesicles (Supplementary Fig. S1A and S1B). In addition, the roots of
278 transgenic *Arabidopsis* expressing SYT1-GFP driven by *SYT1* native promoter and
279 VAP27-1-GFP driven by 35S promoter were stained with the lipophilic styryl dye FM
280 4-64 followed by brefeldin A (BFA) treatment. BFA is a fungal toxin that blocks the
281 secretory vesicle trafficking through the ER and the Golgi apparatus. The blockage
282 will lead to the accumulation of trans-Golgi networks/early endosomes (TGN/EE) and
283 the Golgi apparatus and form the BFA compartments (Berson *et al.*, 2014; Naramoto
284 *et al.*, 2014). The results showed that neither SYT1-GFP nor VAP27-1-GFP was co-
285 localized with the BFA compartments (Supplementary Fig. S1C and S1D), indicating
286 that these two proteins were not incorporated to the endosomes. Cryo-immunogold
287 electron microscopy further confirmed that both SYT1 and VAP27-1 were still
288 localized on the ER-PM contact sites in the BFA-treated root cells (Supplementary
289 Fig. S1E and S1F).

290

291 ***SYT1 and VAP27-1 are localized on different regions of ER-PM contact sites***

292 To examine whether SYT1 and VAP27-1 are localized on the same ER-PM contact
293 sites, SYT1-GFP and VAP27-1-YFP were transiently co-expressed in leaves of
294 *Nicotiana benthamiana*. The result showed that the signal of SYT1-GFP was not
295 completely overlapped with VAP27-1-YFP at EPCSs; however, it was often found
296 localized around VAP27-1-YFP-labeled EPCSs (Fig. 2A, arrows, and Supplementary
297 Movie S2). On the other hand, SYT1-GFP was mainly overlapped with VAP27-1-YFP
298 on the ER strands, tubules or cisternae but not on ER-PM contact sites (Fig. 2A,
299 arrowheads, and Supplementary Movie S2). Statistical analyses showed that 99.17%
300 (476 out of 480) of VAP27-1 puncta were found to be associated with SYT1 puncta
301 whereas only 48.40% (788 out of 1628) of SYT1 puncta were in contact with VAP27-
302 1 puncta (Fig. 2B). It has been shown that over-expression of VAP27-1 and NET3C
303 together in *N. benthamiana* cause the enlargement of the V-EPCSs (Wang *et al.*,
304 2016). To further illustrate the relationships between SYT1, VAP27-1 and NET3C,
305 co-expression of these proteins in tobacco leaves were conducted. Co-expression of

306 STY1-GFP, VAP27-1-YFP and RFP-NET3C showed that VAP27-1-YFP and NET3C-
307 RFP were co-localized on the same ER-PM contact sites, and SYT1-GFP was found
308 closely surround it, little co-localization was observed (Supplementary Fig. S2).
309 Please note that VAP27-1 and NET3C interaction enlarge the size of EPCS as
310 described in (Wang *et al.*, 2016). Previous studies have shown that VAP27-1 interacts
311 with microtubules (Wang *et al.*, 2014) while SYT1 is often excluded by microtubules
312 (Perez Sancho *et al.*, 2015). In order to illustrate the relationships between SYT1,
313 VAP27-1 and the cytoskeletons, co-expression of these proteins and the cytoskeletal
314 markers in *N. benthamiana* leaves were conducted. The results showed that VAP27-1-
315 YFP puncta were often associated with the MBD-MAP4-DsRed-labeled microtubules
316 and in close proximity to the microtubule-depleted region-located SYT1 puncta
317 (Supplementary Fig. S3A). SYT1-GFP puncta are often arranged along the ABD2-
318 mCherry-labeled F-actin (Supplementary Fig. S3B). A VAP27-1 punctum sandwiched
319 by two SYT1 puncta and penetrated by one microtubule is shown in Supplementary
320 Fig. S3A. The aforementioned data indicated that SYT1 might play a role in
321 controlling the formation, the sizes, or the stability of VAP27-1-located EPCSs.

322

323 To obtain more convincing evidence in *Arabidopsis thaliana*, whole-mount
324 immunofluorescent labeling using SYT1- and VAP27-1-specific antibodies (Perez-
325 Sancho *et al.*, 2015; Wang *et al.*, 2014) was conducted to probe the native SYT1 and
326 VAP27-1 proteins in the roots of wild type Arabidopsis. The images showed that
327 SYT1 and VAP27-1 were localized on different regions of the cortical ER (Fig. 3A).
328 Immunofluorescent staining of the root cells in wild type Arabidopsis with SYT1-
329 specific antibody showed clear puncta signals on the cell cortex (Supplementary Fig.
330 S4A) and ER labeling in the cells (Supplementary Fig. S4B). Immunofluorescent
331 labeling in the roots of *SYT1* null mutant, *syt1-2*, with SYT1-specific antibody
332 undergoing the same procedure showed no fluorescent signals (Supplementary Fig.
333 S4C). Western blot using VAP27-1-specific antibody showed a single band of the
334 expected molecular weight in wild-type *Arabidopsis* and SYT1 null mutant. The
335 intensity of the band was reduced in the *VAP27-1* RNAi knockdown line
336 (Supplementary Fig. S4D). These data indicated that the aforementioned antibodies
337 were specific.

338

339 Ultrastructural immunogold labeling for SYT1 (15-nm gold particles) and VAP27-1

340 (6-nm gold particles) further confirmed that these two proteins were localized on
341 distinct domains of the ER-PM contact sites (Fig. 3B). Gold particles located along
342 the PM were counted and the result showed that 61.82% of the labeled regions were
343 VAP27-1 single positive, 28.22% of the labeled regions were SYT1 single positive,
344 and 9.96% of the labeled regions were VAP27-1/SYT1 double positive. Statistical
345 analyses using chi-square test showed that SYT1 and VAP27-1 positive gold particles
346 tended to localize exclusively on distinct domains. SYT1 showed no preference to
347 cluster with SYT1 itself nor with VAP27-1; whereas VAP27-1 tended to cluster with
348 VAP27-1 itself (Table 1). Based on their respective properties, the two distinct ER-PM
349 contact sites were named as SYT1-enriched ER-PM contact sites (S-EPCSs) and
350 VAP27-1-enriched ER-PM contact sites (V-EPCSs).

351

352 *SYT1 stabilizes the V-EPCSs by maintaining the polygonal ER network*

353 Our results showed that SYT1 and VAP27-1 were not co-localized on the ER-PM
354 contact sites. Nevertheless, these two contact sites were closely located; therefore, it
355 was interesting to investigate their anchoring mechanisms. A previous study has
356 shown that point mutations on the MSP domain of VAP27-1 (VAP27-1-T59/60A)
357 reduce the efficiency of PM tethering (Wang *et al.*, 2014). To investigate the
358 localization patterns of VAP27-1 mutant and SYT1, VAP27-1-T59/60A-YFP was co-
359 expressed with SYT1-GFP in tobacco leaves. Time-lapse imaging showed that
360 VAP27-1-T59/60A mutant was distributed on the ER network and unable to form a
361 stable EPCS (Supplementary Fig. S5 and Supplementary Movie S3). Still, the VAP27-
362 1-T59/60A-labeled ER was connected to the stable S-EPCSs (Supplementary Fig. S5
363 and Supplementary Movie S3), indicating that S-EPCSs might restrain the mobility of
364 ER network and VAP27-1. However, the expression of VAP27-1 mutant protein did
365 not affect the stability of S-EPCSs.

366

367 To examine if SYT1 is required for the formation of V-EPCSs, VAP27-1-YFP was
368 stably transformed into Arabidopsis Col-0 and *SYT1* null mutant, *sytl-2*, using floral
369 dipping. The result showed that V-EPCSs still existed in the leaf epidermal cells of
370 *sytl-2*; however, the ER network in *sytl-2* were not well connected and the behavior
371 of the V-EPCSs had changed compared with that in Col-0 background (Fig. 4A).
372 Quantitation of the polygonal network of the ER tubules showed that the number of
373 the three-way junctions was reduced by 70.57% in the leaf cells of *sytl-2* compared

374 with that in Col-0 (Fig. 4B). This result indicated that the cortical ER in *sytl-2* cells
375 was less reticulated. The stable V-EPCSs labeled by VAP27-1-YFP were still recorded
376 in *sytl-2* but showed a 46.61% of reduction in number (Fig. 4C). This result suggested
377 that the establishment and the stability of the V-EPCSs were regulated by SYT1. Less
378 EPCSs could be formed in the absence of SYT1, resulting in a reduced number of
379 three-way junctions.

380

381 To further examine if the dynamic of VAP27-1 on the V-EPCSs was altered in the
382 absence of SYT1, fluorescence recovery after photobleaching (FRAP) of VAP27-1-
383 YFP was performed in the leaves of *VAP27-1-YFP/Col-0* and *VAP27-1-YFP/sytl-2*
384 transgenic *Arabidopsis* (Fig. 5A). The results showed that the maximal recovery of
385 VAP27-1-YFP in *sytl-2* ($69.08\% \pm 2.48\%$) was higher than that in Col-0 ($55.20\% \pm$
386 1.73% , $p\text{-value} < 0.0001$) (Fig. 5B), indicating increased mobility of VAP27-1 in *sytl-*
387 *2*. In addition, 20.69% (12 out of 58) of the V-EPCSs in *sytl-2* were unstable and
388 motile during FRAP analysis compared to only 1.85% (1 out of 54) in Col-0
389 background (Fig. 6 and Supplementary Movie S4), showing that the V-EPCSs were
390 unstable in *SYT1* null mutant. In summary, the above data demonstrate that SYT1 is
391 essential for maintaining the polygonal network of cortical ER and the
392 stability/dynamics of VAP27-1 on the ER-PM contact sites.

393

394 **Discussion**

395 ***Subcellular Localization of SYT1***

396 Early studies suggested SYT1 is a PM protein that can also be found at endosomes
397 (Schapire *et al.*, 2008; Yamazaki *et al.*, 2008; Lewis and Lazarowitz, 2010). However,
398 two recent studies have shown *Arabidopsis* Synaptotagmin 1 is an ER integral membrane
399 protein localized on the ER-PM junctions (Levy *et al.*, 2015; Perez-Sancho *et al.*, 2015).

400 The subcellular localization of *Arabidopsis* SYT1 is convoluted owing to i) the
401 resemblance of the protein to human SYT1 and E-SYT1, ii) the phospholipid binding
402 property of the C2 domains and the characteristic of the transmembrane domain (TM),
403 and iii) the close proximity between the PM and the cortical ER in plant cells.

404 *Arabidopsis* SYT1 was deemed functionally related to human SYT1 because both
405 *Arabidopsis* SYT1 and human SYT1 possess a single N-terminal transmembrane
406 (TM) domain and two tandem C2 domains at the C-terminal. Human E-SYTs,
407 different from *Arabidopsis* SYT1 and human SYT1, have a long N-terminal TM

408 domain that form a hairpin-like structure, and three to five C2 domains at the C-
409 terminals. However, human E-SYTs share with Arabidopsis SYT1 a conserved SMP
410 domain located between their TM and the C2 domains (Kopec *et al.*, 2010; Levy *et al.*,
411 2015). This study demonstrates that Arabidopsis SYT1 is an ER-anchored protein
412 localized on the ER-PM contact sites. Whole-mount fluorescent
413 immunocytochemistry and cryo-immunogold electron microscopy in *Arabidopsis* root
414 tips further confirm the ER-PM localization of AtSYT1. Moreover, no SYT1-positive
415 signal was found on the Golgi apparatus and the BFA compartments, showing that
416 Arabidopsis SYT1 is not transported to the Golgi apparatus. No evidence has
417 suggested that membrane fusion occurs on the ER-PM contact sites in animal cells,
418 even though hemifusion on the ER-chloroplast contact sites has been suggested
419 (Mehrshahi *et al.*, 2013; Prinz, 2014). Therefore, excluding the possibility of transient
420 translocation of Arabidopsis SYT1 from the ER to the PM, Arabidopsis SYT1 is an
421 ER integral membrane protein localized on the ER-PM contact sites.

422

423 Mammalian SYTs and E-SYTs are both highly expressed in neurons; however, the
424 ability of SYTs to translocate through the exocytosis pathway and trigger the
425 membrane fusion makes it functionally different from the ER-retaining E-SYTs.
426 Human E-SYT2 has three C2 domains (C2A-C2B-C2C) and the C2C domain of E-
427 SYT2 is indispensable for the protein's cortical localization and binding to the PM
428 (Giordano *et al.*, 2013). Arabidopsis SYT1, by comparison, contains only two C2
429 domains (C2A-C2B) but is still localized on the cortical ER and tethers to the PM.
430 The SMP domain of Arabidopsis SYT1 has also been shown to be critical for the
431 puncta localization (Yamazaki *et al.*, 2010; Perez-Sancho *et al.*, 2015); however, the
432 deletion of SMP domain in human E-SYT2 has no apparent effect on its localization
433 (Giordano *et al.*, 2013). It seems that Arabidopsis SYTs and mammalian E-SYTs have
434 evolved different sorting and anchoring mechanisms.

435

436 ***Tethering of SYT1 and VAP27-1 on ER-PM Contact Sites***

437 The relationships between Arabidopsis SYT1 and the ER-PM tethering proteins
438 VAP27-1 and NET3C have been addressed in this study. We have confirmed that
439 Arabidopsis SYT1 does not co-localize with VAP27-1 and NET3C on the ER-PM
440 contact sites. The localization patterns of these proteins indicate that there are different
441 types of ER-PM contact sites. These contact sites may have different functions, but their

442 functions are interrelated. From our observation, the V-EPCSs are always associated with
443 the S-EPCSs, but half of the S-EPCSs are not attached to the V-EPCSs, suggesting that
444 the V-EPCSs may be dependent on the S-EPCSs.

445

446 Our results show that the tethering of VAP27-1 to the PM does not require SYT1
447 because the two proteins are not co-localized and the V-EPCSs can still be found in
448 *SYT1* null mutant. However, the ER tubules are more dynamic, the V-EPCSs are less
449 stable, and the turnover of VAP27-1 increases in *SYT1* null mutant. The ER network is
450 less connected and the average number of three-way-junctions is decreased in the
451 absent of SYT1 (Fig. 7), although cells with well-reticulated ER and those with
452 extremely motile ER strands can also be observed in the same leaf. Based on the
453 above observations, it can be inferred that Arabidopsis SYT1 plays important roles in
454 stabilizing the ER network or supporting the compartmentation of the cell cortex.

455

456 ***Patterns of ER-PM Contact Sites and Vesicle Trafficking***

457 Previous studies have indicated that the ER-PM contact sites in nerve cells also
458 display different forms and shapes: the ER-PM junctions show discrete punctate
459 patterns at the synapses, whereas the width of an ER-PM contact site can extend up to
460 2 to 4 μm in other regions of the neurons (Rosenbluth, 1962; Hayashi *et al.*, 2008;
461 Stefan *et al.*, 2013). Moreover, it has been shown that the sizes of the S-EPCSs in
462 Arabidopsis leaf cells are increased by mechanical stress (Perez-Sancho *et al.*, 2015).
463 The expression of SYT1-GFP driven by native *SYT1* promoter in tobacco leaves also
464 shows various patterns and sizes of the S-EPCSs on the cell cortex. The
465 immunofluorescent labeling of SYT1 in the root cells also shows various sizes of the
466 S-EPCS in our observation. The patterns may result from different expression levels
467 of SYT1 and certain regulatory events in the cells.

468

469 A previous study has shown that the formation of PM-derived endosomes is inhibited
470 by the expression of truncated SYT1 lacking the C2B domain in *N. benthamiana* leaf
471 cells (Lewis and Lazarowitz, 2010). Arabidopsis SYT1 has also been shown to
472 participate in plasma membrane resealing (Yamazaki *et al.*, 2008), which is mediated
473 by Ca^{2+} -dependent exocytosis in animal cells (McNeil and Kirchhausen, 2005). In
474 addition, Arabidopsis SYT1 interacts with the PM syntaxin penetration 1 (PEN1) and
475 negatively regulates the immune secretory pathways in response to powdery mildew

476 fungi probably via modulating the ER-PM contact sites (Kim et al., 2016).

477

478 This study has demonstrated that the fluorescence recovery of VAP27-1-YFP after
479 photobleaching on the ER-PM contact sites is enhanced in *SYT1* null mutant. Because
480 the enhanced mobility of VAP27-1 on the V-EPCSs couples with the enhanced ER
481 remodeling in *SYT1* mutant, it can be inferred that Arabidopsis SYT1 restrains the ER
482 movement by ER-PM tethering and then stabilizes the V-EPCSs without a direct
483 interaction with VAP27-1. Taken together, these data suggest that Arabidopsis SYT1
484 play a role in maintaining the ER stability and regulating vesicle trafficking by
485 controlling the extent of ER-PM contact sites. Recently, different types of proteins
486 localized on the ER-PM contact sites have also been discovered in yeast and human
487 (Gatta *et al.*, 2015; Henne *et al.*, 2015). Further studies on ER-PM anchor proteins in
488 plants will help to reveal the complexity of ER-PM interactions.

489

490 **Supplementary Data**

491 **Supplementary Fig. S1. SYT1 and VAP27-1 are not localized to the Golgi**
492 **apparatus and clathrin-coated vesicles.**

493 **Supplementary Fig. S2. NET3C are co-localized with VAP27-1 on the V-EPCSs.**

494 **Supplementary Fig. S3. Spatial relationships between SYT1, VAP27-1, and the**
495 **cytoskeletons.**

496 **Supplementary Fig. S4. SYT1 and VAP27 antibodies are specific.**

497 **Supplementary Fig. S5. VAP27-1-T59/60A does not interrupt the formation of S-**
498 **EPCSs.**

499 **Supplementary Movie S1. Co-expression of SYT1-GFP and RFP-HDEL.**

500 **Supplementary Movie S2. Co-expression of SYT1-GFP and VAP27-1-YFP.**

501 **Supplementary Movie S3. Co-expression of SYT1-GFP and VAP27 mutant-YFP.**

502 **Supplementary Movie S4. The V-EPCSs are more motile in Arabidopsis *SYT1* null**
503 **mutant.**

504

505 **Acknowledgement**

506 We thank Professor Miguel A. Botella (University of Malaga, Spain) for the SYT1
507 specific antibody, and Professor Yukio Kawamura (Iwate University, Japn) for the
508 *SYT-GFP* construct. We also thank Ursula Mettbach (University of Bonn, Germany)
509 for technical assistance on immunogold labeling. This work was kindly supported by

510 German Academic Exchange Service (DAAD).

Reference

- Baluska F, Mancuso S, Volkmann D, Barlow PW.** 2010. Root apex transition zone: a signalling-response nexus in the root. *Trends in Plant Science* **15**, 402-408.
- Batoko H, Zheng H-Q, Hawes C, Moore I.** 2000. A Rab1 GTPase is required for transport between the endoplasmic reticulum and Golgi Apparatus and for normal Golgi movement in plants. *Plant Cell* **12**, 2201-2217.
- Berson T, von Wangenheim D, Takáč T, Šamajová O, Rosero A, Ovečka M, Komis G, Stelzer EHK, Šamaj J.** 2014. Trans-Golgi network localized small GTPase RabA1d is involved in cell plate formation and oscillatory root hair growth. *BMC Plant Biology* **14**, 252.
- Clough SJ, Bent AF.** 1998. Floral dip: a simplified method for *Agrobacterium*-mediated transformation of *Arabidopsis thaliana*. *Plant Journal* **16**, 735-743.
- Craxton M.** 2010. A manual collection of Syt, Esyt, Rph3a, Rph3al, Doc2, and Dblc2 genes from 46 metazoan genomes - an open access resource for neuroscience and evolutionary biology. *BMC Genomics* **11**, 37.
- Deeks MJ, Calcutt JR, Ingle EK, Hawkins TJ, Chapman S, Richardson AC, Mentlak DA, Dixon MR, Cartwright F, Smertenko AP, Oparka K, Hussey PJ.** 2012. A Superfamily of Actin-Binding Proteins at the Actin-Membrane Nexus of Higher Plants. *Current Biology* **22**, 1595-1600.
- Gatta AT, Wong LH, Sere YY, Calderón-Noreña DM, Cockcroft S, Menon AK, Levine TP.** 2015. A new family of StART domain proteins at membrane contact sites has a role in ER-PM sterol transport. *eLife* **4**, e07253.
- Giordano F, Saheki Y, Idevall-Hagren O, Colombo SF, Pirruccello M, Milosevic I, Gracheva EO, Bagriantsev SN, Borgese N, De Camilli P.** 2013. PI(4,5)P₂-dependent and Ca²⁺-regulated ER-PM interactions mediated by the extended synaptotagmins. *Cell* **153**, 1494-1509.
- Granger CL, Cyr RJ.** 2001. Spatiotemporal relationships between growth and microtubule orientation as revealed in living root cells of *Arabidopsis thaliana* transformed with green-fluorescent-protein gene construct GFP-MBD. *Protoplasma* **216**, 201-214.
- Graumann K, Irons SL, Runions J, Evans DE.** 2007. Retention and mobility of the mammalian lamin B receptor in the plant nuclear envelope. *Biology of the Cell* **99**, 553-562.
- Griffing LR, Gao HT, Sparkes I.** 2014. ER network dynamics are differentially

controlled by myosins XI-K, XI-C, XI-E, XI-I, XI-1, and XI-2. *Frontiers in Plant Science* **5**, 218.

Hawkins TJ, Deeks MJ, Wang P, Hussey PJ. 2014. The evolution of the actin binding NET superfamily. *Frontiers in Plant Science* **5**, 254.

Hayashi M, Raimondi A, O'Toole E, Paradise S, Collesi C, Cremona O, Ferguson SM, De Camilli P. 2008. Cell- and stimulus-dependent heterogeneity of synaptic vesicle endocytic recycling mechanisms revealed by studies of dynamin 1-null neurons. *Proceedings of the National Academy of Sciences of the United States of America* **105**, 2175-2180.

Henne WM, Liou J, Emr SD. 2015. Molecular mechanisms of inter-organelle ER–PM contact sites. *Current Opinion in Cell Biology* **35**, 123-130.

Kim H, Kwon H, Kim S, Kim MK, Botella MA, Yun HS, Kwon C. 2016. Synaptotagmin 1 negatively controls the two distinct immune secretory pathways to powdery mildew fungi in Arabidopsis. *Plant and Cell Physiology* **57**, 1133-1141.

Kopec KO, Alva V, Lupas AN. 2010. Homology of SMP domains to the TULIP superfamily of lipid-binding proteins provides a structural basis for lipid exchange between ER and mitochondria. *Bioinformatics* **26**, 1927-1931.

Kriechbaumer V, Botchway SW, Slade SE, Knox K, Frigerio L, Oparka K, Hawes C. 2015. Reticulomics: Protein-Protein Interaction Studies with Two Plasmodesmata-Localized Reticulon Family Proteins Identify Binding Partners Enriched at Plasmodesmata, Endoplasmic Reticulum, and the Plasma Membrane. *Plant Physiology* **169**, 1933-1945.

Lee H, Sparkes I, Gattolin S, Dzimitrowicz N, Roberts LM, Hawes C, Frigerio L. 2013. An Arabidopsis reticulon and the atlastin homologue RHD3-like2 act together in shaping the tubular endoplasmic reticulum. *New Phytologist* **197**, 481-489.

Levy A, Zheng JY, Lazarowitz SG. 2015. Synaptotagmin SYTA forms ER-plasma membrane junctions that are recruited to plasmodesmata for plant virus movement. *Current Biology* **25**, 2018-2025.

Lewis JD, Lazarowitz SG. 2010. Arabidopsis synaptotagmin SYTA regulates endocytosis and virus movement protein cell-to-cell transport. *Proceedings of the National Academy of Sciences of the United States of America* **107**, 2491-2496.

Marc J, Granger CL, Brincat J, Fisher DD, Kao T-h, McCubbin AG, Cyr RJ. 1998. A GFP–MAP4 Reporter Gene for Visualizing Cortical Microtubule Rearrangements in Living Epidermal Cells. *Plant Cell* **10**, 1927-1939.

- McNeil PL, Kirchhausen T.** 2005. An emergency response team for membrane repair. *Nature Reviews Molecular Cell Biology* **6**, 499-505.
- Mehrshahi P, Stefano G, Andaloro JM, Brandizzi F, Froehlich JE, DellaPenna D.** 2013. Transorganellar complementation redefines the biochemical continuity of endoplasmic reticulum and chloroplasts. *Proceedings of the National Academy of Sciences of the United States of America* **110**, 12126-12131.
- Min SW, Chang WP, Sudhof TC.** 2007. E-Syts, a family of membranous Ca²⁺-sensor proteins with multiple C2 domains. *Proceedings of the National Academy of Sciences of the United States of America* **104**, 3823-3828.
- Moghadam PK, Jackson MB.** 2013. The Functional Significance of Synaptotagmin Diversity in Neuroendocrine Secretion. *Frontiers in Endocrinology* **4**, 124.
- Nalefski EA, Falke JJ.** 1996. The C2 domain calcium-binding motif: structural and functional diversity. *Protein Science* **5**, 2375-2390.
- Naramoto S, Otegui MS, Kutsuna N, de Rycke R, Dainobu T, Karampelias M, Fujimoto M, Feraru E, Miki D, Fukuda H, Nakano A, Friml J.** 2014. Insights into the localization and function of the membrane trafficking regulator GNOM ARF-GEF at the Golgi apparatus in Arabidopsis. *Plant Cell* **26**, 3062-3076.
- Perez-Sancho J, Vanneste S, Lee E, McFarlane HE, Esteban Del Valle A, Valpuesta V, Friml J, Botella MA, Rosado A.** 2015. The Arabidopsis synaptotagmin1 is enriched in endoplasmic reticulum-plasma membrane contact sites and confers cellular resistance to mechanical stresses. *Plant Physiology* **168**, 132-143.
- Prinz WA.** 2014. Bridging the gap: membrane contact sites in signaling, metabolism, and organelle dynamics. *The Journal of Cell Biology* **205**, 759-769.
- Renna L, Hanton SL, Stefano G, Bortolotti L, Misra V, Brandizzi F.** 2005. Identification and characterization of AtCASP, a plant transmembrane Golgi matrix protein. *Plant Mol Biol* **58**, 109-122.
- Rosenbluth J.** 1962. Subsurface cisterns and their relationship to the neuronal plasma membrane. *The Journal of Cell Biology* **13**, 405-421.
- Runions J, Brach T, Kuhner S, Hawes C.** 2006. Photoactivation of GFP reveals protein dynamics within the endoplasmic reticulum membrane. *Journal of Experimental Botany* **57**, 43-50.
- Saravanan RS, Slabaugh E, Singh VR, Lapidus LJ, Haas T, Brandizzi F.** 2009. The targeting of the oxysterol-binding protein ORP3a to the endoplasmic reticulum relies on the plant VAP33 homolog PVA12. *Plant Journal* **58**, 817-830.

- Schapiro AL, Voigt B, Jasik J, Rosado A, Lopez-Cobollo R, Menzel D, Salinas J, Mancuso S, Valpuesta V, Baluska F, Botella MA.** 2008. Arabidopsis synaptotagmin 1 is required for the maintenance of plasma membrane integrity and cell viability. *Plant Cell* **20**, 3374-3388.
- Schoberer J, Runions J, Steinkellner H, Strasser R, Hawes C, Osterrieder A.** 2010. Sequential depletion and acquisition of proteins during Golgi stack disassembly and reformation. *Traffic* **11**, 1429-1444.
- Sparkes IA, Runions J, Kearns A, Hawes C.** 2006. Rapid, transient expression of fluorescent fusion proteins in tobacco plants and generation of stably transformed plants. *Nature Protocols* **1**, 2019-2025.
- Stefan CJ, Manford AG, Emr SD.** 2013. ER–PM connections: sites of information transfer and inter-organelle communication. *Current Opinion in Cell Biology* **25**, 434-442.
- Sutter J-U, Campanoni P, Blatt MR, Paneque M.** 2006. Setting SNAREs in a Different Wood. *Traffic* **7**, 627-638.
- Uchiyama A, Shimada-Beltran H, Levy A, Zheng JY, Javia PA, Lazarowitz SG.** 2014. The Arabidopsis synaptotagmin SYTA regulates the cell-to-cell movement of diverse plant viruses. *Frontiers in Plant Science* **5**, 584.
- Voigt B, Timmers ACJ, Šamaj J, Müller J, Baluška F, Menzel D.** 2005. GFP-FABD2 fusion construct allows in vivo visualization of the dynamic actin cytoskeleton in all cells of Arabidopsis seedlings. *European Journal of Cell Biology* **84**, 595-608.
- Wang P, Hawkins TJ, Richardson C, Cummins I, Deeks MJ, Sparkes I, Hawes C, Hussey PJ.** 2014. The plant cytoskeleton, NET3C, and VAP27 mediate the link between the plasma membrane and endoplasmic reticulum. *Current Biology* **24**, 1397-1405.
- Wang L, Li H, Lv X, Chen T, Li R, Xue Y, Jiang J, Jin B, Baluška F, Šamaj J, Wang X, Lin J.** 2015. Spatiotemporal Dynamics of the BRI1 Receptor and its Regulation by Membrane Microdomains in Living Arabidopsis Cells. *Molecular Plant* **8**, 1334-1349.
- Wang P, Hummel E, Osterrieder A, Meyer AJ, Frigerio L, Sparkes I, Hawes C.** 2011. KMS1 and KMS2, two plant endoplasmic reticulum proteins involved in the early secretory pathway. *Plant Journal* **66**, 613-628.
- Wang P, Richardson C, Hawkins TJ, Sparkes I, Hawes C, Hussey PJ.** 2016. Plant

VAP27 proteins: domain characterization, intracellular localization and role in plant development. *New Phytologist* **210**, 1311–1326.

Wang Q, Zhao Y, Luo W, Li R, He Q, Fang X, Michele RD, Ast C, von Wirén N, Lin J. 2013. Single-particle analysis reveals shutoff control of the Arabidopsis ammonium transporter AMT1;3 by clustering and internalization. *Proceedings of the National Academy of Sciences of the United States of America* **110**, 13204-13209.

Yamazaki T, Kawamura Y, Minami A, Uemura M. 2008. Calcium-dependent freezing tolerance in Arabidopsis involves membrane resealing via synaptotagmin SYT1. *Plant Cell* **20**, 3389-3404.

Yamazaki T, Takata N, Uemura M, Kawamura Y. 2010. Arabidopsis synaptotagmin SYT1, a type I signal-anchor protein, requires tandem C2 domains for delivery to the plasma membrane. *Journal of Biological Chemistry* **285**, 23165-23176.

Zhang X, Henriques R, Lin SS, Niu QW, Chua NH. 2006. Agrobacterium-mediated transformation of Arabidopsis thaliana using the floral dip method. *Nature Protocols* **1**, 641-646.

Table

Table 1. Statistical Analysis for clustering of gold particles. 15-nm (SYT1) and 6-nm (VAP27-1) gold particles are counted along the PM. A 100x50 nm area with positive signal(s) is defined as one labeled ER-PM contact site. The contact sites are designated as SYT1 positive (SYT1+), VAP27-1 positive (VAP27+), and SYT1/VAP27-1 double positive (SYT1+VAP27+). Chi-square tests show that SYT1 particles are randomly distributed on the SYT1+ and SYT1+VAP27+ contact sites, but VAP27-1 particles tend to clusters together on VAP27+ contact sites. The values in parentheses indicate expected values of random distribution.

ER-PM Contact Sites Labeled by Gold Particles					
	SYT1+	SYT1+VAP27+	VAP27+	Total	
No. of Contact Sites	68	24	149	241	
χ^2 test for Clustering of Gold Particles					p-value
No. of SYT1 particles	161 (156.70)	51 (55.20)	–	212	0.5
No. of VAP27-1 particles	–	77 (124.86)	823 (775.14)	900	3.93E-06

Figure Legends

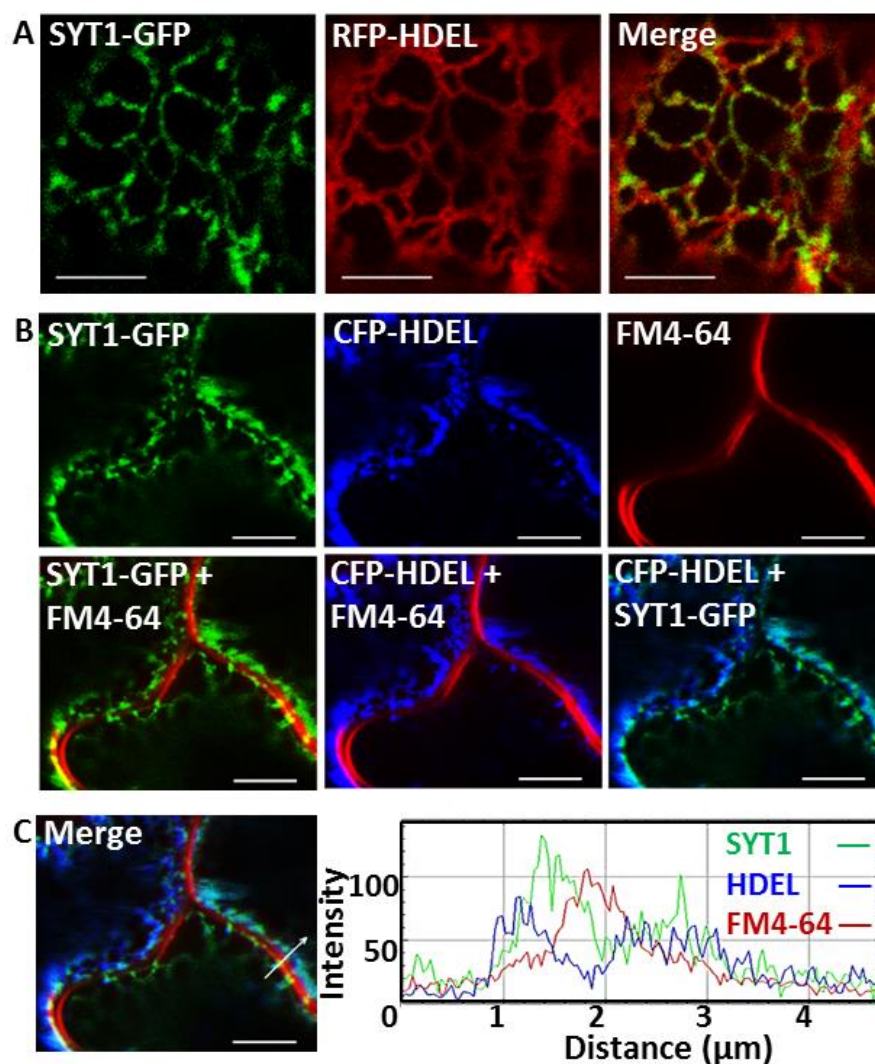


Fig. 1. SYT1 unevenly distributes on the cortical ER and forms stable attachment to the PM in *N. benthamiana* leaf epidermis. (A) Co-expression of SYT1-GFP and RFP-HDEL shows that the stable SYT1 puncta are localized on ER tubules and cisternae. (B) ER-resident SYT1 attaches to the FM4-64-stained PM at the immotile ER-PM contact sites. (C) The intensity profiles of the cells in (B) show that SYT1 signal peaks between the ER lumen marker HDEL and the PM marker FM4-64 at the ER-PM contact sites. Scale bars = 5 μm

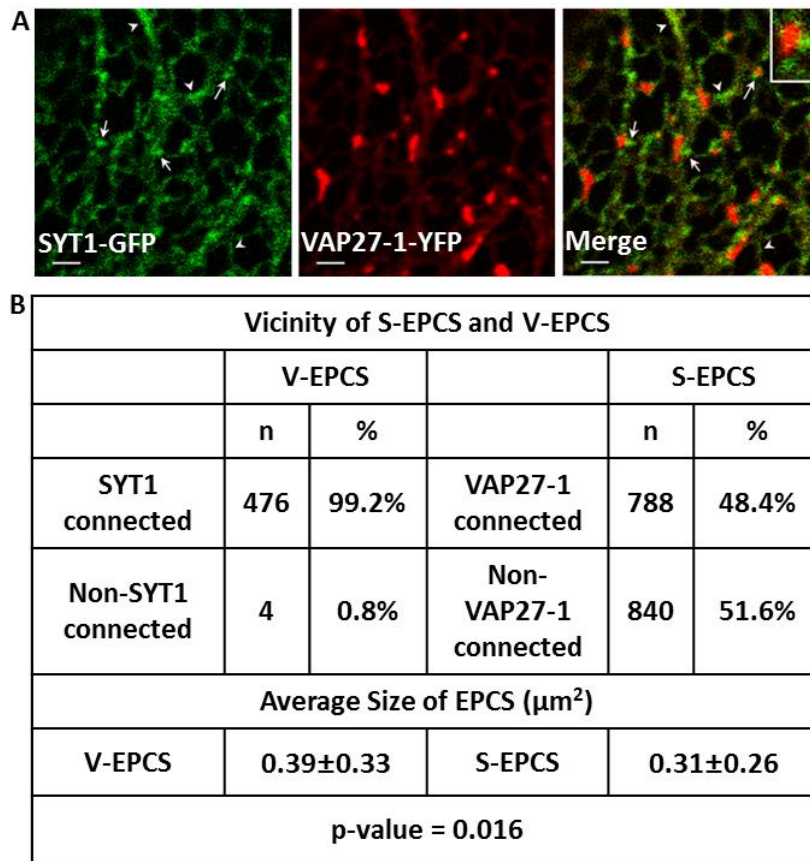


Fig. 2. SYT1 and VAP27-1 are localized on different regions of ER-PM contact sites in *N. benthamiana* leaf epidermis. (A) The VAP27-1-enriched ER-PM contact sites (V-EPCSs) do not overlaps with the SYT1-enriched ER-PM contact sites (S-EPCSs) (arrows). SYT1 partly overlaps with VAP27-1 on the motile ER tubules or strands (arrowheads). The inset shows a V-EPCS surrounded by the S-EPCSs. Scale bar = 2 μm . (B) Spatial relationship between S-EPCSs and V-EPCSs. Almost all V-EPCSs are in contact with S-EPCSs, but about half of S-EPCSs are localized on the ER without connection with V-EPCSs. The average size of V-EPCS is slightly larger than that of S-EPCS; however, the sizes of EPCSs vary wildly from cells to cells as indicated by the high standard deviations (\pm SD). 16 cells from 3 independent experiments are analyzed.

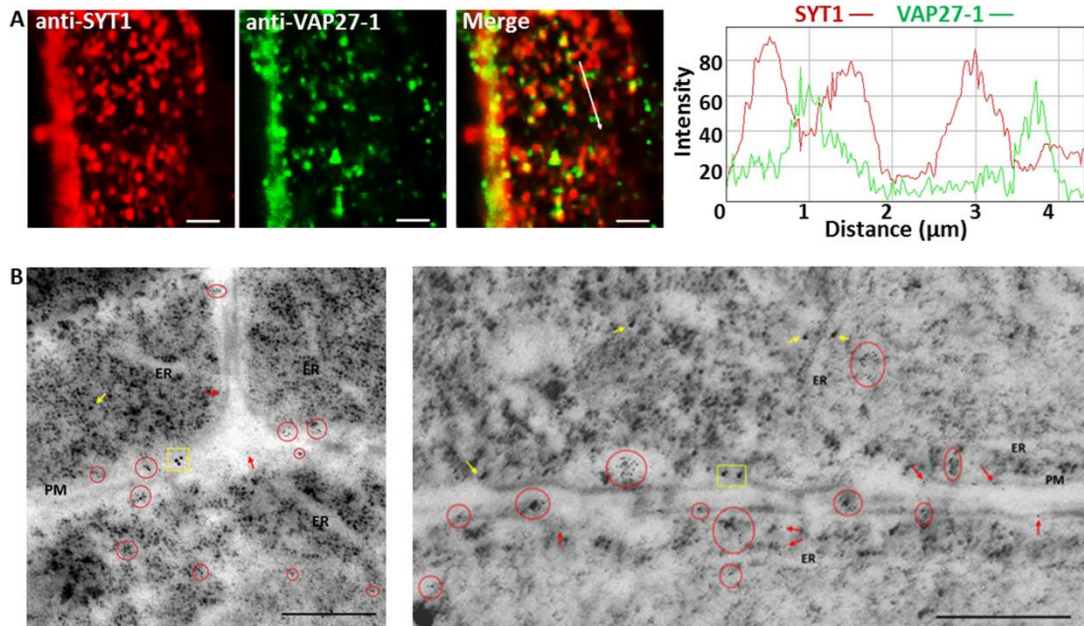


Fig. 3. SYT1 and VAP27-1 accumulate on different regions of the ER-PM contact sites in *Arabidopsis* root cells. (A) Whole-mount immunocytochemistry of the root cells in wild type *Arabidopsis* shows that SYT1 and VAP27-1 puncta are in close vicinity on the cell cortex. The intensity profiles show that the peaks of SYT1 and VAP27-1 signals are shifted. Scale bars = 2 μm . (B) Double Immunogold labeling of SYT1 and VAP27-1 in *Arabidopsis* roots. The electron micrographs of ultrathin cryosections of wild type *Arabidopsis* root cells and immunogold labeling show that SYT1 (15-nm gold particles) and VAP27-1 (6-nm gold particles) are not localized on the same regions along the PM. The clusters of gold particles are highlighted as SYT1-clusters (yellow rectangles) and VAP27-1-clusters (red circles). SYT1 single labeling (yellow arrows) and VAP27-1 single labeling (red arrows) are indicated. Scale bars = 500 nm.

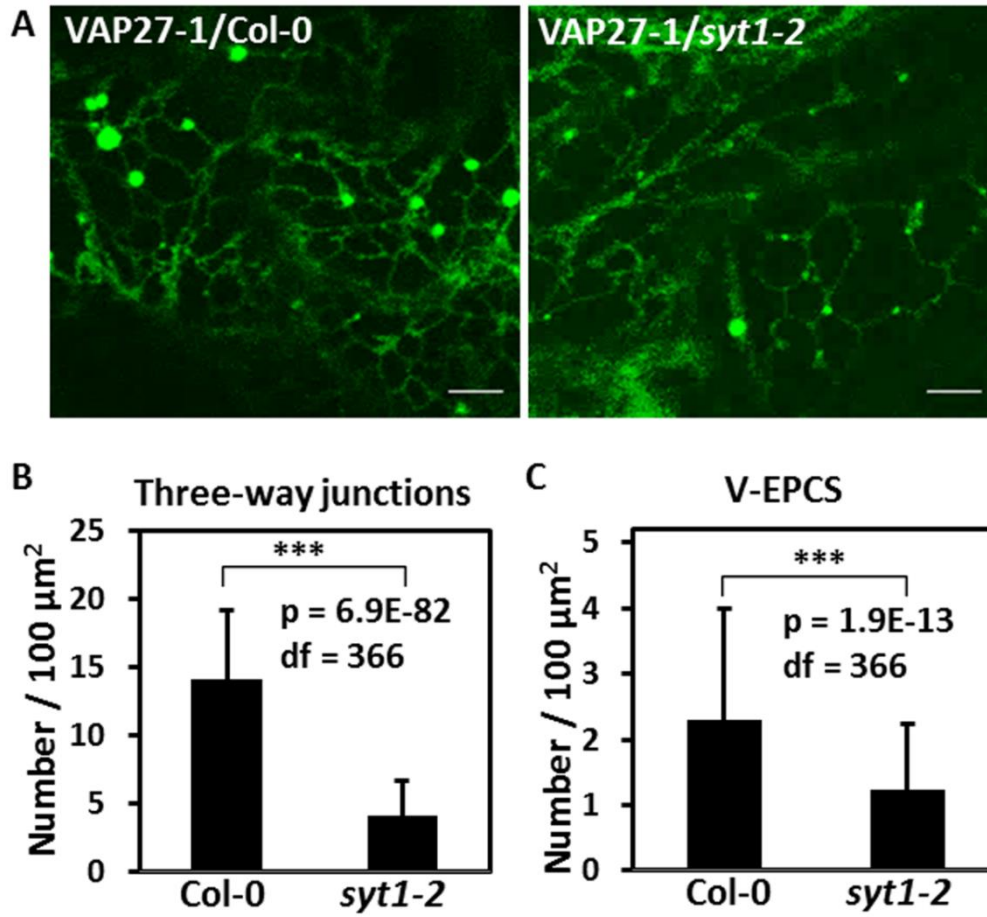


Fig. 4. SYT1 is essential for maintaining the polygonal network of ER. (A) The stable VAP27 puncta are still observed in the leaf cells of VAP27-YFP transgenic *Arabidopsis* in *syt1-2* background, but the ER network in *syt1-2* background is less connected compared with that in Col-0 background. (B) Comparing the number of the three-way junctions of the ER in the leaf cells of VAP27-YFP/Col-0 and VAP27-YFP/*syt1-2* transgenic *Arabidopsis* shows that the junctions is significantly reduced in *syt1-2* background. (t-test, p-value < 0.001***). (C) The number of the VECSs is reduced by 46.61% in the loss of SYT1. (t-test, p-value < 0.001**). The three-way junctions and the V-EPCSs were counted per 100 μm² in the first leaf cells of the transgenic plants from the confocal images. In total, 368 of the areas from 64 cells were counted. Scale bars = 5 μm. Error bars = standard deviation (SD). (This figure is available in colour at JXB online.)

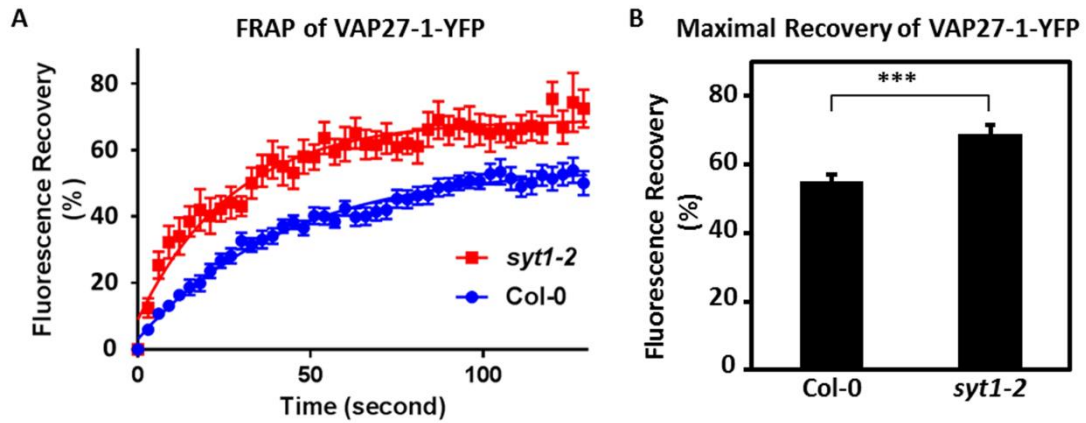


Fig. 5. The motility of VAP27-1 at the ER-PM contact sites is restrained by SYT1. (A) FRAP of VAP27-1-YFP at the VECSs in the leaf cells of VAP27-1-YFP/Col-0 and VAP27-1-YFP/*syt1-2* transgenic *Arabidopsis* shows that the maximal recovery of VAP27-1-YFP in *syt1-2* background is higher than that in Col-0 background. Note that the error bars are wider in *syt1-2* background, indicating that the recovery of VAP27 is more various. Error bars = standard error of the mean (SE). (B) The diagram shows that the motile fraction of VAP27 is enhanced in the absence of SYT1. The three asterisks indicate significant difference between the two groups according to the extra-sum-of-squares F test of the best-fit values (p-value < 0.0001). 13 VECSs of each line were analyzed. Error bars = 95% confidence intervals. (This figure is available in colour at JXB online.)

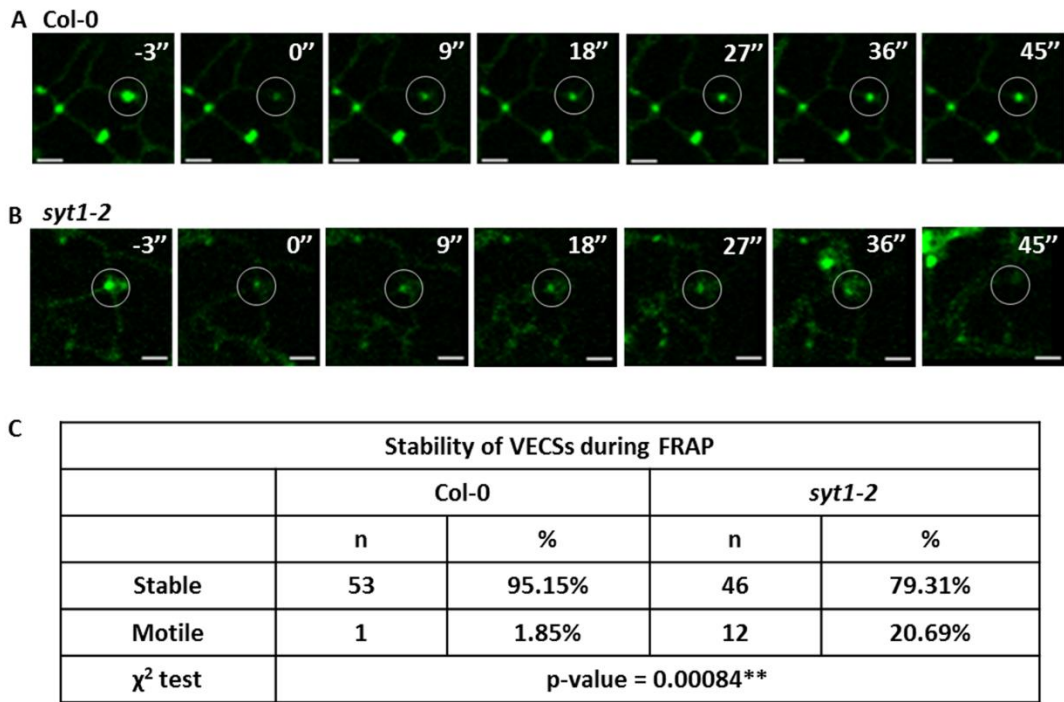


Fig. 6. The VAP27-enriched ER-PM contact sites are unstable in the absence of SYT1. (A) Time-lapse images show that the fluorescence of VAP27-YFP is able to recovery at the same spot in Col-0 background. 0'' indicates the first captured image after photobleaching. Scale bars = 2 μ m. (B) Time-lapse images show one example that a VAP27-YFP punctum moves away while recording the movies in *syt1-2* background. (C) Chi-squared tests show that there are more unsteady VAP27 puncta in *syt1-2* null background.

(This figure is available in colour at JXB online.)

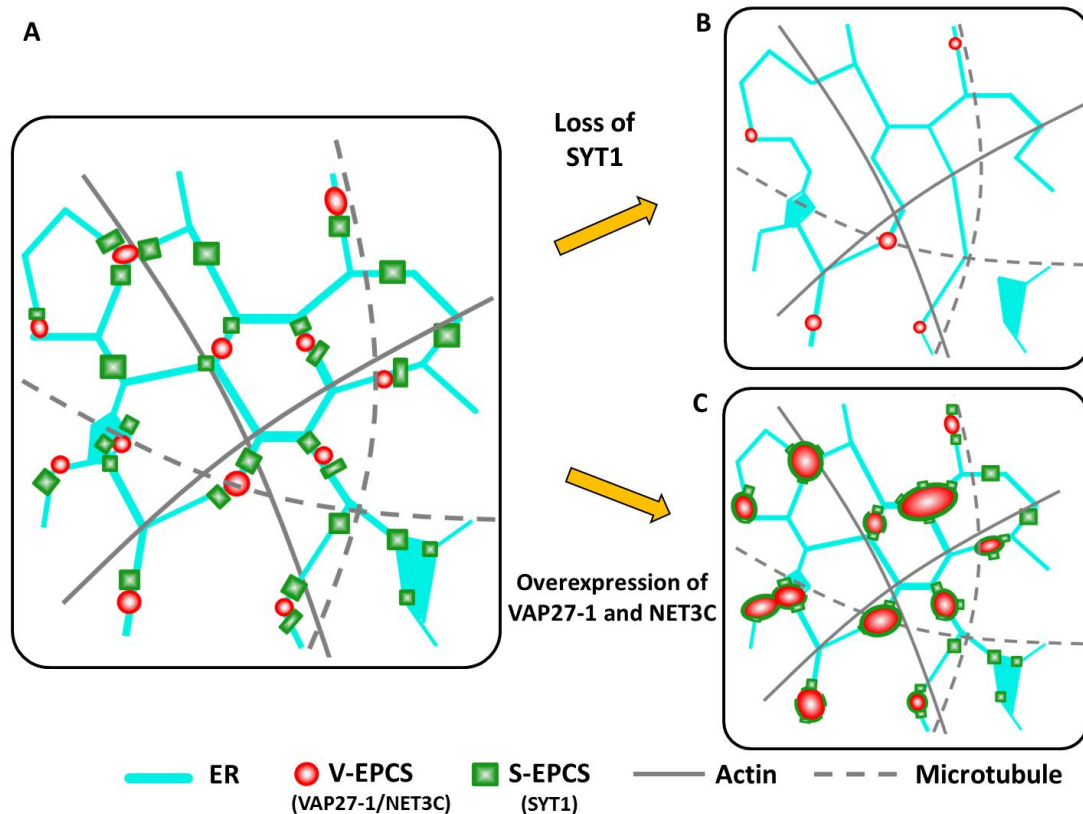


Fig. 7. Schematic of SYT1, VAP27-1, NET3C and cytoskeletons on the cortical ER. (A) VAP27-1 and NET3C are co-localized on the V-EPCSs, which are surrounded by the S-EPCSs. SYT1 maintains the polygonal network of cortical ER and the stability of V-EPCSs by tethering the ER to the PM. S-EPCSs are often arranged along the actin filament but tend to be excluded by the microtubules. ER-resident VAP27-1 interacts with NET3C and microtubules whereas NET3C interacts with VAP27-1, ER and PM membranes, and actin on the V-EPCSs. Therefore, the V-EPCSs are stabilized by microtubules, NET3C and S-EPCSs on the cortical ER. (B) The absence of SYT1 protein results in a less stable and reticulated ER network, fewer V-EPCSs, and less stability of VAP27-1 on the V-EPCSs. The reduced stability of ER network and the EPCSs may give rise to the stress-sensitive phenotypes in *SYT1* null mutant. (C) Overexpression of VAP27-1 and/or NET3C results in the enlargement of the V-EPCSs, which are encircled by the S-EPCSs. In this model, Arabidopsis ER-PM contact sites can be characterized by a central VAP27-1/NET3C core (V-EPCS) and the SYT1 periphery (S-EPCSs). SYT1 may play roles in creating and maintaining the boundaries of the ER-PM contact sites.

(This figure is available in colour at JXB online.)